Front. Struct. Civ. Eng. 2021, 15(6): 1494–1503
https://doi.org/10.1007/s11709-021-0768-y

RESEARCH ARTICLE

Effect of interface adhesion factor on the bearing capacity of strip footing placed on cohesive soil overlying rock mass

Shuvankar DAS, Debarghya CHAKRABORTY*

Department of Civil Engineering, Indian Institute of Technology Kharagpur, Kharagpur 721302, India
**Corresponding author. E-mail: debarghya@civil.iitkgp.ac.in*

ABSTRACT The problem related to bearing capacity of footing either on pure soil or on pure rock mass has been investigated over the years. Currently, no study deals with the bearing capacity of strip footing on a cohesive soil layer overlying rock mass. Therefore, by implementing the lower bound finite element limit analysis in conjunction with the second-order cone programming and the power cone programming, the ultimate bearing capacity of a strip footing located on a cohesive soil overlying rock mass is determined in this study. By considering the different values of interface adhesion factor (α_{cr}) between the cohesive soil and rock mass, the ultimate bearing capacity of strip footing is expressed in terms of influence factor (I_f) for different values of cohesive soil layer cover ratio (T_{cs}/B). The failure of cohesive soil is modeled by using Mohr−Coulomb yield criterion, whereas Generalized Hoek−Brown yield criterion is utilized to model the rock mass at failure. The variations of I_f with different magnitudes of α_{cr} are studied by considering the influence of the rock mass strength parameters of beneath rock mass layer. To examine stress distribution at different depths, failure patterns are also plotted.

KEYWORDS bearing capacity, soil-rock interface, Hoek−Brown yield criterion, plasticity, limit analysis

1 Introduction

Soil layer generally deposits over the bedrock layer. It was found in several cases that topsoil layers are cohesive in nature. Most researches related to bearing capacity determination were accomplished by considering the foundation on cohesive soil [1–4] or pure rock deposits [5–8]. In addition, the effect of layer soil in the bearing capacity determination of strip footing was also examined by researchers [9–12]. Recently, Ouahab et al. [13] investigated the bearing capacity of strip footing on a cohesive soil layer overlying a rigid base. However, to the knowledge of these authors, there is no study dealing with the bearing capacity of strip footing on a cohesive soil layer overlying rock mass. Thus, the bearing capacity of strip footing placed on cohesive soil overlying rock mass is determined in this study. Failure in cohesive soil is generally modeled by using Mohr−Coulomb (MC) yield criterion [14], whereas Generalized Hoek−Brown (GHB) yield criterion [15] is well accepted for modeling rock mass. By implementing the finite element limit analysis method, it is possible to estimate the collapse load in a bracketed form, i.e., the upper and lower bound collapse load. Among these, a conservative and safe collapse load can be predicted by using the lower bound finite element limit analysis (LBFELA). Most importantly, no assumption is considered for the geometry of the collapse mechanism in the LBFELA. For this reason, the present study implements the LBFELA technique. Here, the LBFELA in conjunction with two conic optimization techniques, namely second-order cone programming (SOCP) and power cone programming (PCP), are utilized to model MC and GHB yield criteria, respectively. Additionally, cohesive soil−rock interface is taken into account in this study. Recently, Halder and Chakraborty [16] anticipated a generalized outline for the frictional soil-reinforcement interface friction angle in the LBFELA. Formulation of Halder and Chakraborty [16] is modified and applied in this study in an effort to consider the effect of developed adhesion in the cohesive soil−rock

Article history: Received Mar 18, 2021; Accepted Jul 28, 2021

interface. Effects of thickness of the soil layer (T_{cs}), rock mass strength parameters (GSI, m_i, D), and cohesive soil-rock adhesion factors (α_{cr}) are examined in detail. Additionally, the extent of the failure zone during collapse is examined in an effort to understand failure mechanism.

2 Problem definition

A rough strip footing of width B, as shown in Fig. 1(a), is located on a cohesive soil overlying a rock mass. A vertical compressive load (Q_u) is present in the strip footing. MC and GHB yield criteria are utilized to model

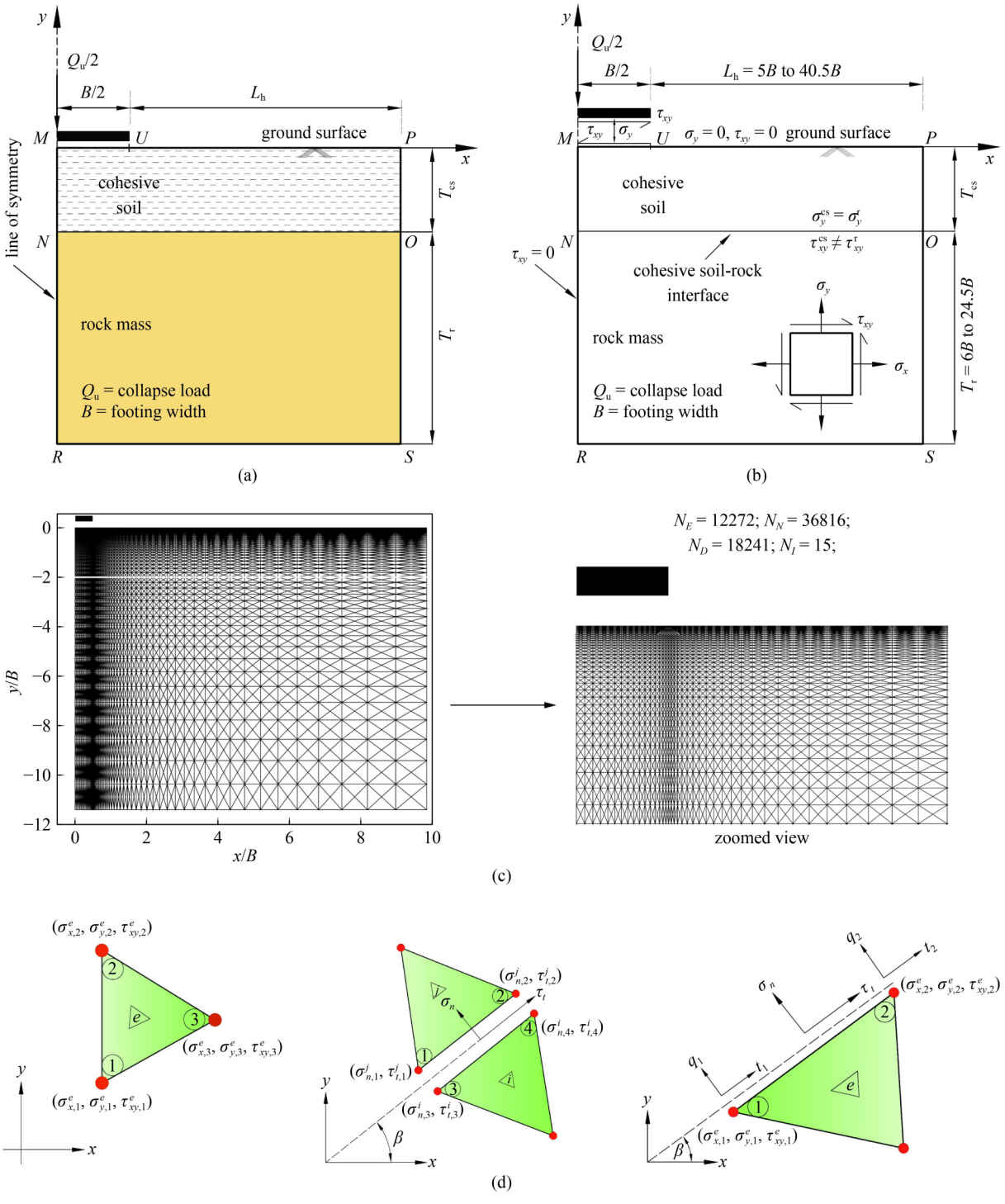

Fig. 1 (a) Problem definition; (b) chosen domain and stress boundary conditions; (c) finite element mesh used in the analysis along with zoomed view around the footing for $\phi = 0°$, $\alpha_{cr} = 1$, $GSI = 30$, $m_i = 25$, $D = 0$, $\sigma_{ci}/\gamma B = \infty$, $T_{cs}/B = 2$; (d) triangular element, stress discontinuity between two triangular elements, and boundary condition in the LBFELA.

the failure of cohesive soil and rock mass, respectively. This study is intended to evaluate ultimate bearing capacity of strip footing for various magnitudes of soil layer thickness to footing width ratio (T_{cs}/B) by considering various values of the cohesive soil-rock adhesion factor (α_{cr}).

3 Mesh and boundary details

Two-dimensional plane strain domain with associated stress boundary conditions is illustrated in Fig. 1(b). Shear stress along the vertical boundary (*MR*) are considered as zero. Additionally, shear and normal stresses are considered as zero along the horizontal ground surface (*UP*). Because the footing base-soil interface is considered as rough, no boundary condition is implemented along *MU*. The shear strength of cohesive soil, by default, controls the stresses on this boundary. The thickness of cohesive soil layer, T_{cs} is varied for different depths to determine the collapse load. The thickness of rock layer (T_r) below the cohesive soil layer and the horizontal extent (L_h) of the ground surface are selected in such a manner that 1) rock mass elements on boundary edges (*PS* and *RS*) do not yield, and 2) the magnitude of collapse load does not depend on selected size of the domain. Triangle elements having three nodes are utilized to discretise the selected problem domain. A study regarding mesh convergence is performed to inspect the effect of mesh types on the magnitude of efficiency factor, I_f, as presented in Table 1. Five types of mesh (very coarse, coarse, medium, fine, and very fine) are utilized based on the number of elements. By comparing the magnitude of I_f, there is a negligible difference between fine and very fine mesh. In addition, comparatively, more computational time is required for the case of very fine mesh. Therefore, fine type mesh is utilized to carry out the analysis. A typical finite element mesh having $\phi = 0°$, $\alpha_{cr} = 1$, $GSI = 30$, $m_i = 25$, $D = 0$, $\sigma_{ci}/\gamma B = \infty$, and $T_{cs}/B = 2$ is illustrated in Fig. 1(c), where the total number of nodes, elements, discontinuities, and nodes along the footing base are described by N_N, N_E, N_D, and N_I, respectively.

4 Methodology

The plane strain LBFELA formulation of Sloan [17] is utilized to perform the analysis. Therefore, at each node of triangular elements, there are three unknown nodal stresses, σ_x, σ_y, and τ_{xy} (Fig. 1(d)). The value of maximum collapse load (objective function) is determined by employing equality and inequality constraints in the problem domain. These constraints arise from the satisfaction of 1) the equilibrium equations at all the elements, 2) the stress boundary conditions, 3) stress discontinuity across the edges of two adjacent elements, and 4) the yield criterion. Two different conic programming techniques, namely SOCP and PCP, are applied at the nodes of the same problem domain to implement the well accepted MC yield criterion for cohesive soil [18] and GHB yield criterion for rock mass [7], respectively. In addition, the existence of interface adhesion between cohesive soil and rock mass are also investigated. In this study, a brief discussion of GHB yield criterion and detailed expressions regarding interface formulation are provided below.

4.1 Generalized Hoek−Brown yield criterion

GHB yield criterion [15] is employed in this study to model the collapse of rock mass and can be expressed in this form:

$$\sigma_1 - \sigma_3 - \left(-(\sigma_{ci})^{\left(\frac{1}{\alpha}-1\right)} m_b \sigma_1 + s(\sigma_{ci})^{\frac{1}{\alpha}}\right)^{\alpha} \leqslant 0, \qquad (1)$$

where σ_1 and σ_3 are effective major and minor principal stresses, m_b, s, and α are the functions of Geological Strength Index (*GSI*), material constant (m_i), and disturbance factor (*D*). In this study, normal tensile stress is viewed as positive. The above parameters are calculated using the following relationships:

$$m_b = m_i \exp\left(\frac{GSI - 100}{28 - 14D}\right), \qquad (2a)$$

$$s = \exp\left(\frac{GSI - 100}{9 - 3D}\right), \qquad (2b)$$

$$\alpha = \frac{1}{2} + \frac{1}{6}\left(e^{-\frac{GSI}{15}} - e^{-\frac{20}{3}}\right), \qquad (2c)$$

where *GSI* varies from 10 (poor rock mass) to 100 (intact

Table 1 Mesh convergence study for a rough strip footing placed on cohesive soil overlying rock mass having $T_{cs}/B = 0.5$, $GSI = 30$, $m_i = 5$, $D = 0$, $\sigma_{ci}/\gamma B = \infty$, and $\alpha_{cr} = 1$

different parameters	type of mesh				
	very coarse	coarse	medium	fine	very fine
number of elements	2223	5919	7273	10825	13793
efficiency factor, I_f	0.912	0.920	0.924	0.931	0.932
required CPU time for the analysis (s)	10.06	40.93	55.19	85.17	127.18

rock mass); m_i varies between 1 and 35; D varies from 0 (undisturbed rock mass) to 1 (highly disturbed rock mass).

4.2 Cohesive soil-rock interface

To incorporate interface effect within formulation, discontinuity in the shear stress and continuity in the normal stress is considered between adjacent elements along the cohesive soil−rock interface. Expressions for shear stress (τ_t) and normal stress (σ_n) acting on a plane having an angle β with horizontal are written as:

$$\tau_t = -0.5\sigma_x \sin 2\beta + 0.5\sigma_y \sin 2\beta + \tau_{xy} \cos 2\beta, \tag{3a}$$

$$\sigma_n = \sigma_x \sin^2\beta + \sigma_y \cos^2\beta - \tau_{xy} \sin 2\beta. \tag{3b}$$

Therefore, considering the above, two new constraints equations are formulated along the cohesive soil−rock interface and expressed in the matrix form as:

$$[A_{dc}^{sr}]\{\sigma_{dc}\} = \{b_{dc}^{sr}\}, \tag{4a}$$

where

$$[A_{dc}^{sr}] = \begin{bmatrix} P & -P & 0 & 0 \\ 0 & 0 & P & -P \end{bmatrix}, \tag{4b}$$

$$[P] = [\ \sin^2\beta \quad \cos^2\beta \quad -\sin 2\beta\ ], \tag{4c}$$

$$\{b_{dc}^{sr}\}^T = \begin{Bmatrix} 0 & 0 \end{Bmatrix}, \tag{4d}$$

$$\{\sigma_{dc}\}^T = \{\sigma_{x,1} \quad \sigma_{y,1} \quad \tau_{xy,1} \quad \sigma_{x,2} \quad \sigma_{y,2} \quad \tau_{xy,2} \quad \sigma_{x,3} \quad \sigma_{y,3} \quad \tau_{xy,3} \quad \sigma_{x,4} \quad \sigma_{y,4} \quad \tau_{xy,4}\}. \tag{4e}$$

In this study, except for cohesive soil−rock interface, four constraints equations are applied in the discontinuity edges of the problem domain and written as:

$$[A_{dc}^{st}]\{\sigma_{dc}\} = \{b_{dc}^{st}\}, \tag{5a}$$

where

$$[A_{dc}^{st}] = \begin{bmatrix} R & -R & 0 & 0 \\ 0 & 0 & R & -R \end{bmatrix}, \tag{5b}$$

$$[R] = \begin{bmatrix} \sin^2\beta & \cos^2\beta & -\sin 2\beta \\ -0.5\sin 2\beta & 0.5\sin 2\beta & \cos 2\beta \end{bmatrix}, \tag{5c}$$

$$\{b_{dc}^{st}\}^T = \begin{Bmatrix} 0 & 0 & 0 & 0 \end{Bmatrix}. \tag{5d}$$

The effect of developed cohesive soil−rock interface adhesion (A_{cr}) is considered in this study, by introducing different values of cohesive soil−rock interface adhesion factor ($\alpha_{cr} = \dfrac{A_{cr}}{c}$). The effect of the cohesive soil−rock interface is examined by considering the variation of α_{cr} between 0 and 1. In the formulation, it is ensured that shear stress of the top cohesive soil layer does not cross the shear strength of cohesive soil. This assumption tends to generate two constraints equations along nodes of the cohesive soil−rock interface and may be written as:

$$|\tau_{xy}| \leqslant \alpha_{cr} c, \tag{6a}$$

$$[A_{int,i}^{sr}]\{\sigma_{int,i}\} = \{b_{int,i}^{sr}\}, \tag{6b}$$

where

$$[A_{int,i}^{sr}] = \begin{bmatrix} 0 & 0 & -1 \\ 0 & 0 & 1 \end{bmatrix}, \tag{6c}$$

$$\{b_{int,i}^{sr}\} = \begin{Bmatrix} c\alpha_{cr} \\ c\alpha_{cr} \end{Bmatrix}, \tag{6d}$$

$$\{\sigma_{int,i}\} = \begin{Bmatrix} \sigma_{x,i} \\ \sigma_{y,i} \\ \tau_{xy,i} \end{Bmatrix}. \tag{6e}$$

In Eqs. (6b) and (6e), $\{\sigma_{int,i}\}$ is stress vectors containing stresses for nodes located along the soil side of the cohesive soil−rock interface. Other than the discontinuity constraints equations, the equilibrium, boundary, and yield constraints equations are also implemented in the problem domain. To avoid repetitions, these formulations are not discussed. One can refer Sloan [17], Makrodimopoulos and Martin [18], and Kumar and Rahaman [7] for detailed formulation on equilibrium, boundary, and yield conditions.

4.3 Final form of the optimization problem

All constraints equations are expressed in matrix form and assembled in a manner which allows one to solve the problem by using SOCP and PCP. The final form of the present optimization problem is written as:

$$\text{maximize} \begin{Bmatrix} c_{obj}^T \end{Bmatrix} \{\bar{z}\}, \tag{7a}$$

$$\text{subjected to } [A]\{\bar{z}\} = \{b\}, \tag{7b}$$

$$f(\bar{z}) \leqslant 0, \tag{7c}$$

where $\{c_{obj}^T\}$is the global vector comprising coefficients of objective function; $\{\bar{z}\}$ is the global vector of unknown stresses including auxiliary variables; $f(\bar{z})$ is the function having global inequality constraint associated with yield criteria; $[A]$ and $\{b\}$ are the global matrix and vector of

the constraints, respectively. A computer code is developed and executed in MATLAB [19] to perform an analysis by using LBFELA formulation with the SOCP and PCP by employing primal-dual interior-point solver, MOSEK [20]. Previously, several studies [18,21–25] implemented MOSEK to solve SOCP optimization issues. Conversely, a limited number of current studies [7,26] have applied MOSEK to solve PCP optimization problems.

5 Results and comparison

5.1 Variation of I_f

Influence factor (I_f) is defined as the ratio of bearing capacity of footing placed on cohesive soil overlying rock mass, to bearing capacity of footing placed only on cohesive soil. Variation of the magnitude of I_f is obtained as a series of design charts (Figs. 2−4) by varying T_{cs}/B between 0.25 and 8; α_{cr} between 0 and 1; *GSI* value between 10 and 100; m_i value between 5 and 35; D value between 0 and 1 for a weightless ($\sigma_{ci}/\gamma B = \infty$) rock mass.

In this study, relative increase in the magnitude of I_f can be observed with the increase in α_{cr} value for all cases. The value of I_f increases gradually to unity with the increase of T_{cs}/B value for an underneath rock mass having lower *GSI* and m_i values, as shown in Figs. 2(a)−2(e), 3(a)−3(g), 3(i), 4(a)−4(j). For relatively higher value of *GSI* having α_{cr} = 0.8, and 1, it is observed that the magnitude of I_f decreases to unity with the increase of T_{cs}/B. While rock mass having the relatively higher value of *GSI* and α_{cr} = 0, 0.2, 0.4, and 0.6, the magnitude of I_f decreases to a particular value and then increases to the unity with the increase of T_{cs}/B, as shown in Figs. 2(f)−2(g), 3(h), 3(j)−3(k), 4(l)−4(m). It can also be found that the magnitude of I_f reaches to the unity at relatively lower T_{cs}/B value with the increase in α_{cr} value. In contrast, the value of I_f reaches to the unity at relatively higher T_{cs}/B value with the increase in the magnitude of D, as shown in Figs. 2−4.

5.2 Comparison

For validation, a rigid strip footing placed on cohesive soil (ϕ = 0º) without any underlying rock mass is considered. The presently obtained magnitude of bearing

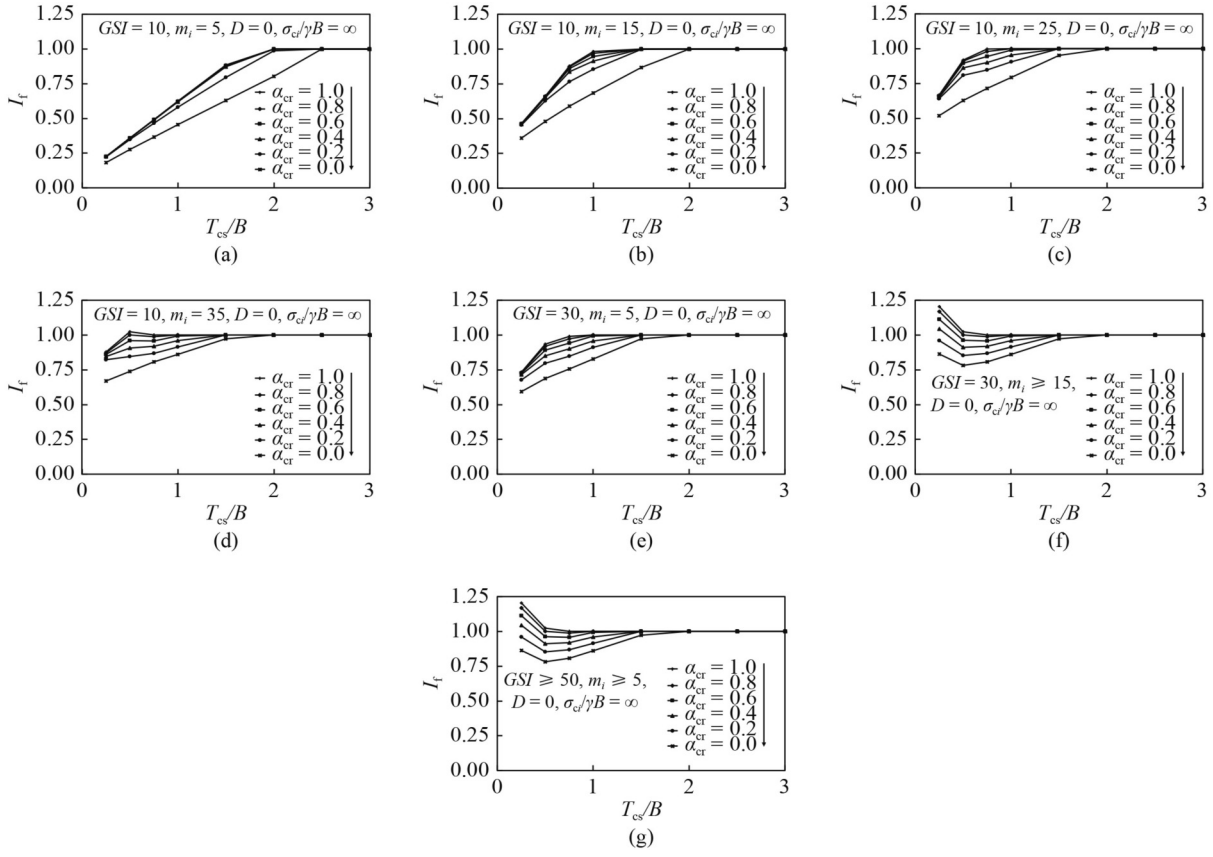

Fig. 2 Variation of influence factor (I_f) for: (a) *GSI* = 10, m_i = 5, D = 0, $\sigma_{ci}/\gamma B = \infty$; (b) *GSI* = 10, m_i = 15, D = 0, $\sigma_{ci}/\gamma B = \infty$; (c) *GSI* = 10, m_i = 25, D = 0, $\sigma_{ci}/\gamma B = \infty$; (d) *GSI* = 10, m_i = 35, D = 0, $\sigma_{ci}/\gamma B = \infty$; (e) *GSI* = 30, m_i = 5, D = 0, $\sigma_{ci}/\gamma B = \infty$; (f) *GSI* = 30, $m_i \geqslant 15$, D = 0, $\sigma_{ci}/\gamma B = \infty$; (g) *GSI* $\geqslant$ 50, $m_i \geqslant 5$, D = 0, $\sigma_{ci}/\gamma B = \infty$.

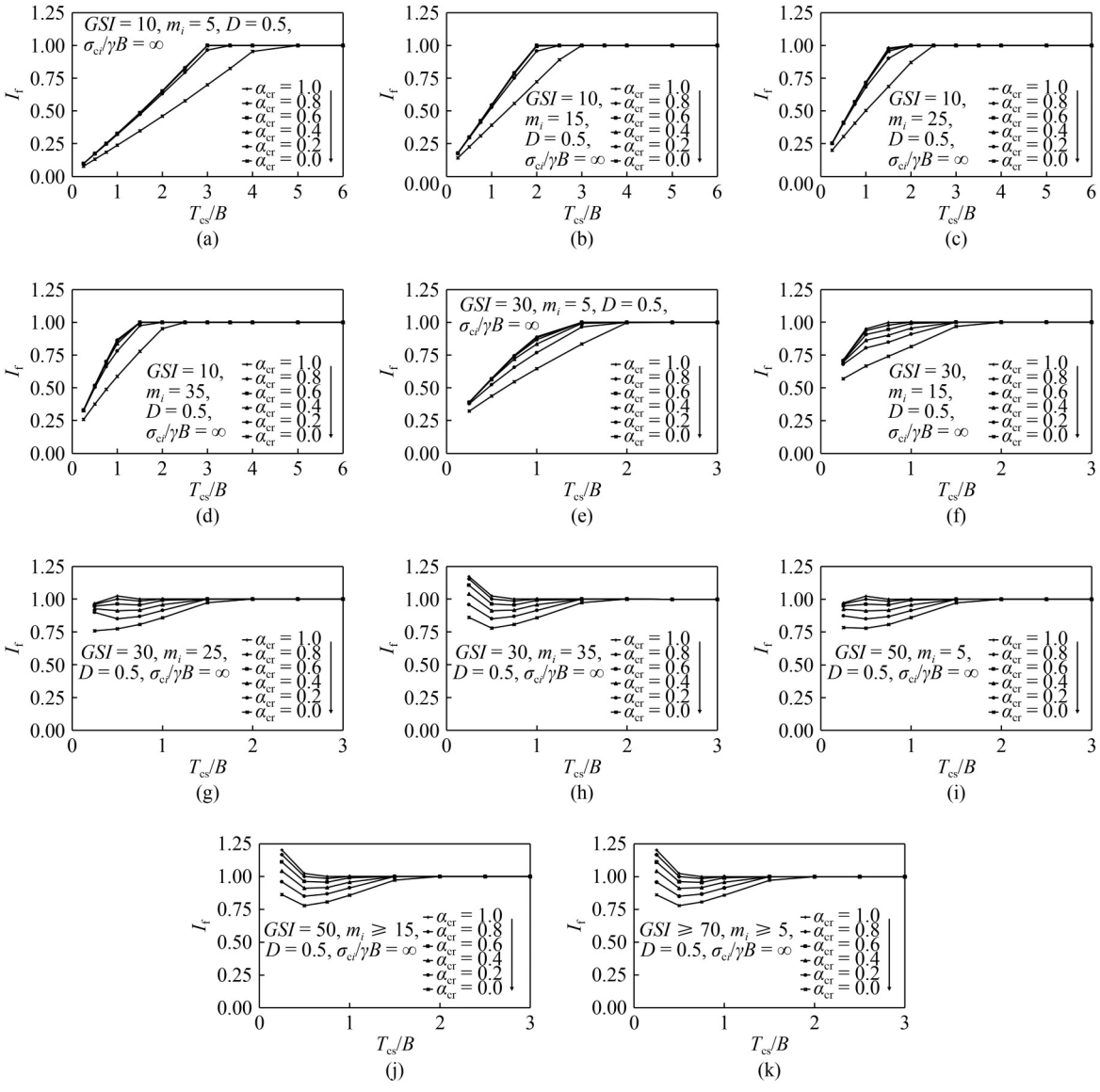

Fig. 3 Variation of influence factor (I_f) for: (a) $GSI = 10$, $m_i = 5$, $D = 0.5$, $\sigma_{ci}/\gamma B = \infty$; (b) $GSI = 10$, $m_i = 15$, $D = 0.5$, $\sigma_{ci}/\gamma B = \infty$; (c) $GSI = 10$, $m_i = 25$, $D = 0.5$, $\sigma_{ci}/\gamma B = \infty$; (d) $GSI = 10$, $m_i = 35$, $D = 0.5$, $\sigma_{ci}/\gamma B = \infty$; (e) $GSI = 30$, $m_i = 5$, $D = 0.5$, $\sigma_{ci}/\gamma B = \infty$; (f) $GSI = 30$, $m_i = 15$, $D = 0.5$, $\sigma_{ci}/\gamma B = \infty$; (g) $GSI = 30$, $m_i = 25$, $D = 0.5$, $\sigma_{ci}/\gamma B = \infty$; (h) $GSI = 30$, $m_i = 35$, $D = 0.5$, $\sigma_{ci}/\gamma B = \infty$; (i) $GSI = 50$, $m_i = 5$, $D = 0.5$, $\sigma_{ci}/\gamma B = \infty$; (j) $GSI = 50$, $m_i \geqslant 15$, $D = 0.5$, $\sigma_{ci}/\gamma B = \infty$; (k) $GSI \geqslant 70$, $m_i \geqslant 5$, $D = 0.5$, $\sigma_{ci}/\gamma B = \infty$.

capacity factor ($N_c = \dfrac{Q_u}{cB}$) is compared with 1) the elastoplastic finite element analysis solution of Griffiths [9], 2) limit equilibrium solution of Meyerhof [2], and 3) LBFELA in conjunction with linear programming solution of Chakraborty and Kumar [27]. The comparison is presented in Table 2. It is observed that N_c value matches with above-mentioned studies.

There are no studies available for strip footing located on cohesive soil overlying rock mass. However, in recent past, using PLAXIS software, Ouahab et al. [13] determined the bearing capacity of strip footing located on cohesive soil overlying bedrock, which was modeled as a rigid material. More significantly, Ouahab et al. [13] did not consider the influences of the rock mass strength parameters (GSI, m_i, D) of the beneath rock mass layer and the interface adhesion factor (α_{cr}). Therefore, strip footing having different values of GSI, m_i, D, α_{cr} =1 and $\sigma_{ci}/\gamma B = \infty$ is considered, and the obtained influence factor (I_f) is compared with the solution of Ouahab et al. [13], as shown in Fig. 5. One must note, the magnitude of I_f is slightly lower than the values described by Ouahab et al. [13] for relatively strong rock. Additionally, the trend of obtained magnitude of I_f matches with the solution of Ouahab et al. [13] for a rock mass having relatively higher GSI, m_i, and lower D values. Alternatively, it was found that a significant effect of rock mass strength parameters is present on the magnitude of I_f for a strip footing located on the cohesive soil overlying relatively

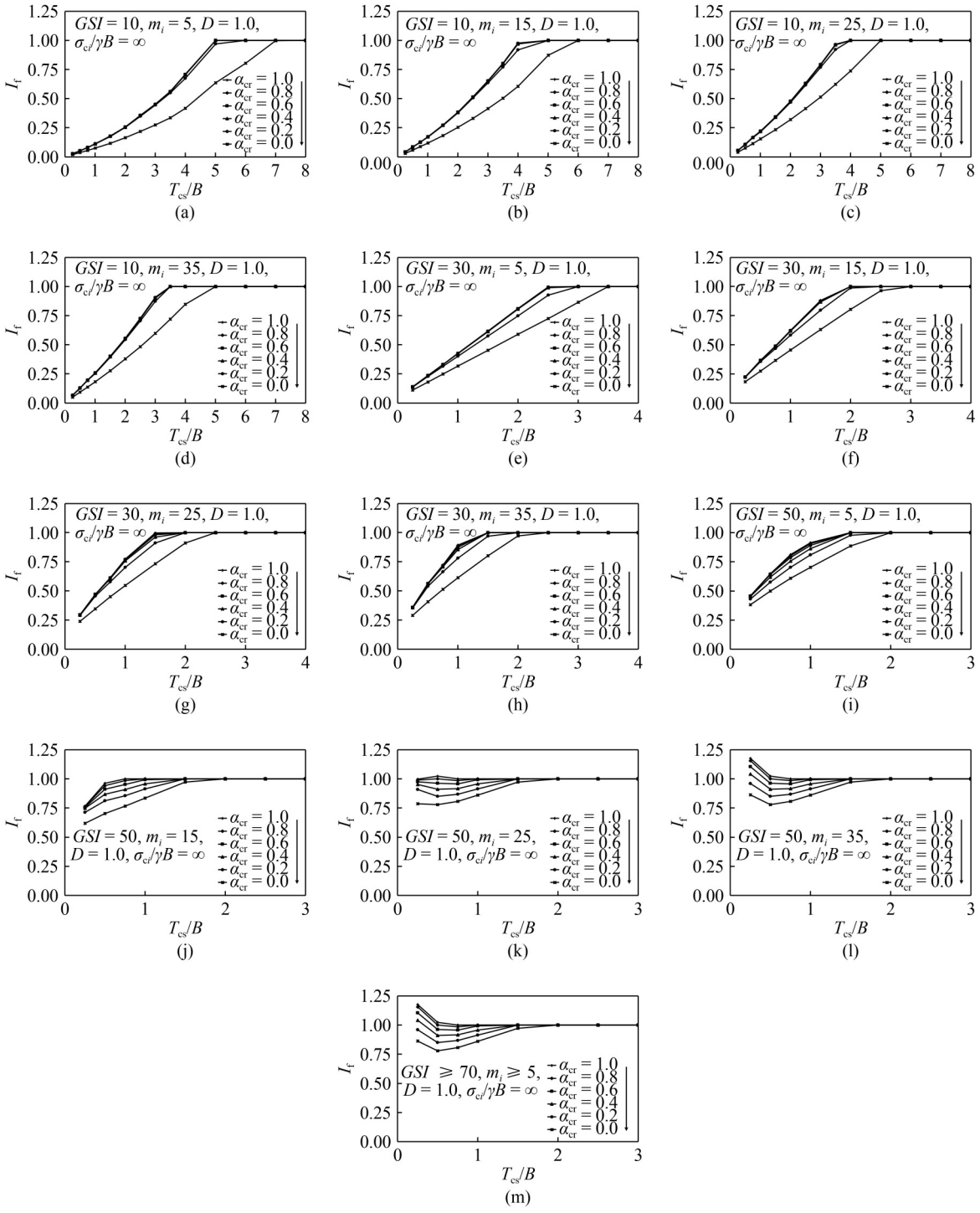

Fig. 4 Variation of influence factor (I_f) for: (a) $GSI = 10$, $m_i = 5$, $D = 0.5$, $\sigma_{ci}/\gamma B = \infty$; (b) $GSI = 10$, $m_i = 15$, $D = 0.5$, $\sigma_{ci}/\gamma B = \infty$; (c) $GSI = 10$, $m_i = 25$, $D = 0.5$, $\sigma_{ci}/\gamma B = \infty$; (d) $GSI = 10$, $m_i = 35$, $D = 0.5$, $\sigma_{ci}/\gamma B = \infty$; (e) $GSI = 30$, $m_i = 5$, $D = 0.5$, $\sigma_{ci}/\gamma B = \infty$; (f) $GSI = 30$, $m_i = 15$, $D = 0.5$, $\sigma_{ci}/\gamma B = \infty$; (g) $GSI = 30$, $m_i = 25$, $D = 0.5$, $\sigma_{ci}/\gamma B = \infty$; (h) $GSI = 30$, $m_i = 35$, $D = 0.5$, $\sigma_{ci}/\gamma B = \infty$; (i) $GSI = 50$, $m_i = 5$, $D = 0.5$, $\sigma_{ci}/\gamma B = \infty$; (j) $GSI = 50$, $m_i = 15$, $D = 0.5$, $\sigma_{ci}/\gamma B = \infty$; (k) $GSI = 50$, $m_i = 25$, $D = 0.5$, $\sigma_{ci}/\gamma B = \infty$; (l) $GSI = 50$, $m_i = 35$, $D = 0.5$, $\sigma_{ci}/\gamma B = \infty$; (m) $GSI \geqslant 70$, $m_i \geqslant 5$, $D = 1.0$, $\sigma_{ci}/\gamma B = \infty$.

weak rock mass. Therefore, it indicates that the influences of the rock mass strength parameters (GSI, m_i, D) of beneath rock mass layer and interface adhesion factor (α_{cr}) is needed to be considered for a rock mass having relatively lower GSI, m_i, and higher D values.

5.3 Failure patterns

Failure patterns for the footing with different thicknesses of soil layer (T_{cs}) and different values α_{cr} are illustrated in Fig. 6. By using a non-dimensional ratio a_1/d_1, the state of

Table 2 Comparison of bearing capacity factor, N_c for rough strip footing placed on cohesive soil without any underlying rock mass

ϕ	present study[a)]	Meyerhof [2][b)]	Griffiths [4][c)]	Chakraborty and Kumar [27][d)]
0	5.13	5.14	5.10	5.09

Notes: a) LBFELA with second order cone programming; b) limit equilibrium method; c) elastoplastic finite element; d) LBFELA with linear programming.

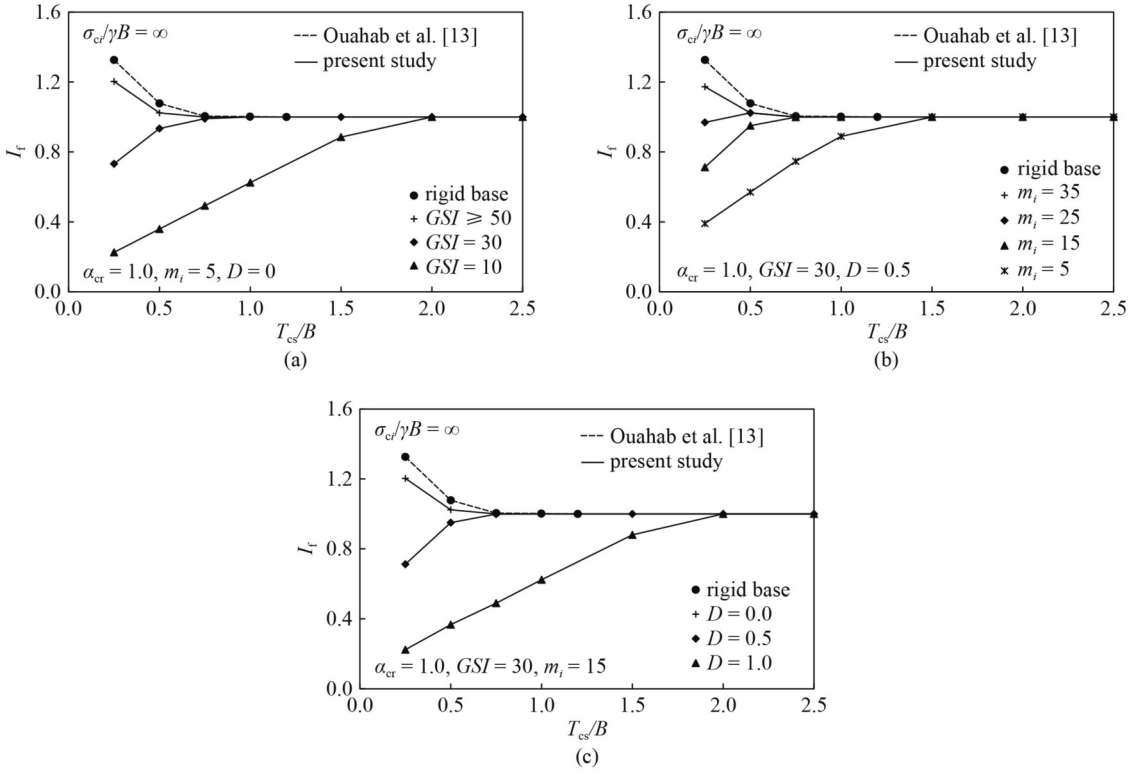

Fig. 5 Comparison of obtained influence factor (I_f) with the result of Ouahab et al. [13] for (a) *GSI* having $m_i = 5$, $D = 0$; (b) m_i having $GSI = 30$, $D = 0.5$; (c) D having $GSI = 30$, $m_i = 15$.

stress at each node is expressed for cohesive soil; where $a_1 = (\sigma_x - \sigma_y)^2 + (2\tau_{xy})^2$, and $d_1 = 4c^2$. Alternatively, the state of stress at each node for rock mass is expressed by a ratio, a_2/d_2, where $a_2 = (\sigma_1 - \sigma_3)$ and $d_2 = \sigma_{ci}(-m_b\frac{\sigma_1}{\sigma_{ci}} + s)^{\alpha}$. For a point at plastic state, the values of a_1/d_1 and a_2/d_2 become unity; on the other hand, $a_1/d_1 < 0$ and $a_2/d_2 < 0$ indicate the non-plastic state. Figures 6(a)–6(i) illustrate the failure patterns for T_{cs}/B = 0.5 and 3, having $GSI = 30$ and 50, $m_i = 5$, $\sigma_{ci}/\gamma B = \infty$ and α_{cr} = 0, 0.4, and 1.0. It can be clearly visible that at a lower value of T_{cs}/B, the plastic zone propagates to the rock mass layer and increases gradually with the increase of the value of α_{cr}, as shown in Figs. 6(a)–6(c). Whereas, with the increase of the values of T_{cs}/B and α_{cr}, the plastic flow confines within the cohesive soil layer only. Additionally, at lower values of T_{cs}/B and α_{cr} = 0, the plastic flow can be found within the top cohesive soil layer (Figs. 6(a) and 6(d)), which indicates sliding of top cohesive soil layer along the cohesive soil-rock interface. The effect of the magnitude of D is shown in Figs. 6(j)–6(l).

6 Remarks

Although by using the LBFELA, the safe collapse load is determined for the strip footing placed on the cohesive soil overlying rock mass, the presently obtained failure mechanisms needs more comprehensive studies by using other numerical methods such as the Phase Field Model (PFM) [28–32]. Therefore, the present problem can be investigated in the future by adopting PFM for the failure mechanisms in soils and rocks.

7 Conclusions

This study aims to provide general guidelines for strip footing in the existence of cohesive soil-rock interface. Thus, the bearing capacity of strip footing placed on cohesive soil overlying rock mass is investigated in terms of influence factor (I_f) by considering various values of cohesive soil−rock adhesion factor and rock mass parameters. Effects of different parameters are also investigated, and results are presented as design charts. It

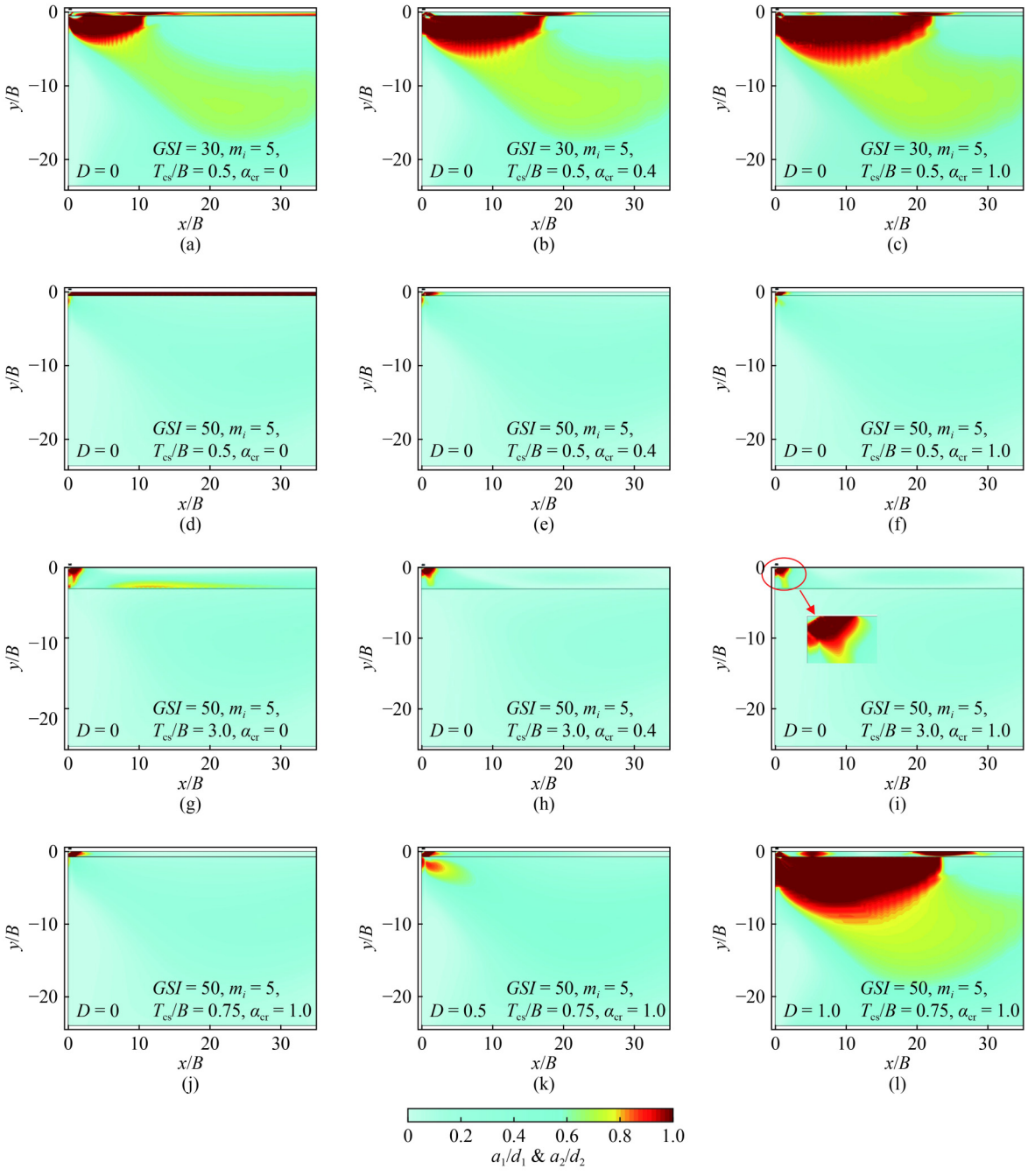

Fig. 6 Failure patterns obtained for: (a) $\phi = 0°$, $GSI = 30$, $m_i = 5$, $D = 0$, $\sigma_{ci}/\gamma B = \infty$, $T_{cs}/B = 0.5$, $\alpha_{cr} = 0$; (b) $\phi = 0°$, $GSI = 30$, $m_i = 5$, $D = 0$, $\sigma_{ci}/\gamma B = \infty$, $T_{cs}/B = 0.5$, $\alpha_{cr} = 0.4$; (c) $\phi = 0°$, $GSI = 30$, $m_i = 5$, $D = 0$, $\sigma_{ci}/\gamma B = \infty$, $T_{cs}/B = 0.5$, $\alpha_{cr} = 1.0$; (d) $\phi = 0°$, $GSI = 50$, $m_i = 5$, $D = 0$, $\sigma_{ci}/\gamma B = \infty$, $T_{cs}/B = 0.5$, $\alpha_{cr} = 0$; (e) $\phi = 0°$, $GSI = 50$, $m_i = 5$, $D = 0$, $\sigma_{ci}/\gamma B = \infty$, $T_{cs}/B = 0.5$, $\alpha_{cr} = 0.4$; (f) $\phi = 0°$, $GSI = 50$, $m_i = 5$, $D = 0$, $\sigma_{ci}/\gamma B = \infty$, $T_{cs}/B = 0.5$, $\alpha_{cr} = 1.0$; (g) $\phi = 0°$, $GSI = 50$, $m_i = 5$, $D = 0$, $\sigma_{ci}/\gamma B = \infty$, $T_{cs}/B = 3.0$, $\alpha_{cr} = 0$; (h) $\phi = 0°$, $GSI = 50$, $m_i = 5$, $D = 0$, $\sigma_{ci}/\gamma B = \infty$, $T_{cs}/B = 3.0$, $\alpha_{cr} = 0.4$; (i) $\phi = 0°$, $GSI = 50$, $m_i = 5$, $D = 0$, $\sigma_{ci}/\gamma B = \infty$, $T_{cs}/B = 3.0$, $\alpha_{cr} = 1.0$; (j) $\phi = 0°$, $GSI = 50$, $m_i = 5$, $D = 0$, $\sigma_{ci}/\gamma B = \infty$, $T_{cs}/B = 0.75$, $\alpha_{cr} = 1.0$; (k) $\phi = 0°$, $GSI = 50$, $m_i = 5$, $D = 0.5$, $\sigma_{ci}/\gamma B = \infty$, $T_{cs}/B = 0.75$, $\alpha_{cr} = 1.0$; (l) $\phi = 0°$, $GSI = 50$, $m_i = 5$, $D = 1.0$, $\sigma_{ci}/\gamma B = \infty$, $T_{cs}/B = 0.75$, $\alpha_{cr} = 1.0$.

is observed that for all cases with the increase of α_{cr} value, the magnitude of I_f increases. In most cases of undisturbed rock mass it was found that the magnitude of I_f becomes unity at $T_{cs}/B > 2$. Adversely, it was found that the magnitude of I_f becomes unity at a much higher T_{cs}/B value for disturbed weak rock mass. Design charts presented in this study would likely be beneficial for practicing engineers.

References

1. Prandtl L. The bond strength of plastic building materials and the

strength of cutting edges. Journal of Applied Mathematics and Mechanics, 1921, 1(1): 15−20
2. Meyerhof G G. Some recent research on the bearing capacity of foundations. Canadian Geotechnical Journal, 1963, 1(1): 16−26
3. Hansen J B. A revised and extended formula for bearing capacity. Bulletin of Danish Geotechnical Institute, 1970, 28: 5−11
4. Griffiths D V. Computation of bearing capacity factors using finite elements. Geotechnique, 1982, 32(3): 195−202
5. Merifield R S, Lyamin A V, Sloan S W. Limit analysis solutions for the bearing capacity of rock masses using the generalised Hoek–Brown criterion. International Journal of Rock Mechanics and Mining Sciences, 2006, 43(6): 920−937
6. Kumar J, Mohapatra D. Lower-bound finite elements limit analysis for Hoek−Brown materials using semidefinite programming. Journal of Engineering Mechanics, 2017, 143(9): 04017077
7. Kumar J, Rahaman O. Lower bound limit analysis using power cone programming for solving stability problems in rock mechanics for generalized Hoek–Brown criterion. Rock Mechanics and Rock Engineering, 2020, 53(7): 3237−3252
8. Das S, Halder K, Chakraborty D. Bearing capacity of interfering strip footings on rock mass. Geomechanics and Geoengineering, 2021: 1−13
9. Griffiths D V. Computation of bearing capacity on layered soils. In: Numerical Methods in Geomechanics, Proceedings of the 4th International Conference. Edmonton: Balkema, 1982: 163−170
10. Florkiewicz A. Upper bound to bearing capacity of layered soils. Canadian Geotechnical Journal, 1989, 26(4): 730−736
11. Burd H J, Frydman S. Bearing capacity of plane-strain footings on layered soils. Canadian Geotechnical Journal, 1997, 34(2): 241−253
12. Huang M, Qin H L. Upper-bound multi-rigid-block solutions for bearing capacity of two-layered soils. Computers and Geotechnics, 2009, 36(3): 525−529
13. Ouahab M Y, Mabrouki A, Mellas M, Benmeddour D. Effect of load eccentricity on the bearing capacity of strip footings on non-homogenous clay overlying bedrock. Transportation Infrastructure Geotechnology, 2018, 5(2): 169−186
14. Mohr O. Circumstances that cause the elastic limit and the breakage of a material. Journal of the German Engineers Association, 1900, 46: 1572−1577 (in German)
15. Hoek E, Carranza-Torres C, Corkum B. Hoek−Brown failure criterion—2002 edition. Proceedings of NARMS-Tac, 2002, 1(1): 267−273
16. Halder K, Chakraborty D. Effect of interface friction angle between soil and reinforcement on bearing capacity of strip footing placed on reinforced slope. International Journal of Geomechanics, 2019, 19(5): 06019008
17. Sloan S W. Lower bound limit analysis using finite elements and linear programming. International Journal for Numerical and Analytical Methods in Geomechanics, 1988, 12(1): 61−77
18. Makrodimopoulos A, Martin C M. Lower bound limit analysis of cohesive-frictional materials using second-order cone programming. International Journal for Numerical Methods in Engineering, 2006, 66(4): 604−634
19. MATLAB. Version 8.5. Natick, Massachusetts: MathWorks. 2015
20. MOSEK ApS. Version 9.0. Copenhagen: MOSEK, 2020
21. Krabbenhøft K, Lyamin A V, Sloan S W. Formulation and solution of some plasticity problems as conic programs. International Journal of Solids and Structures, 2007, 44(5): 1533−1549
22. Tang C, Phoon K K, Toh K C. Lower-bound limit analysis of seismic passive earth pressure on rigid walls. International Journal of Geomechanics, 2014, 14(5): 04014022
23. Nguyen-Xuan H, Rabczuk T. Adaptive selective ES-FEM limit analysis of cracked plane-strain structures. Frontiers of Structural and Civil Engineering, 2015, 9(4): 478−490
24. Ukritchon B, Keawsawasvong S. Lower bound limit analysis of an anisotropic undrained strength criterion using second-order cone programming. International Journal for Numerical and Analytical Methods in Geomechanics, 2018, 42(8): 1016−1033
25. Halder K, Chakraborty D. Probabilistic bearing capacity of strip footing on reinforced soil slope. Computers and Geotechnics, 2019, 116: 103213
26. Rahaman O, Kumar J. Stability analysis of twin horse-shoe shaped tunnels in rock mass. Tunnelling and Underground Space Technology, 2020, 98: 103354
27. Chakraborty D, Kumar J. Bearing capacity of strip foundations in reinforced soils. International Journal of Geomechanics, 2014, 14(1): 45−58
28. Zhou S, Zhuang X, Zhu H, Rabczuk T. Phase field modelling of crack propagation, branching and coalescence in rocks. Theoretical and Applied Fracture Mechanics, 2018, 96: 174−192
29. Zhou S, Rabczuk T, Zhuang X. Phase field modeling of quasi-static and dynamic crack propagation: COMSOL implementation and case studies. Advances in Engineering Software, 2018, 122: 31−49
30. Zhou S, Zhuang X, Rabczuk T. A phase-field modeling approach of fracture propagation in poroelastic media. Engineering Geology, 2018, 240: 189−203
31. Zhuang X, Zhou S, Sheng M, Li G. On the hydraulic fracturing in naturally-layered porous media using the phase field method. Engineering Geology, 2020, 266: 105306
32. Zhou S, Zhuang X, Rabczuk T. Phase-field modeling of fluid-driven dynamic cracking in porous media. Computer Methods in Applied Mechanics and Engineering, 2019, 350: 169−198